Dooley, K.L. et al. (2016) GEO 600 and the GEO-HF upgrade program: successes and challenges. Classical and Quantum Gravity, 33(7), 075009.

http://eprints.gla.ac.uk/123900/

Deposited on: 19 September 2016

GEO 600 and the GEO-HF upgrade program: successes and challenges

K L Dooley[1,10]**, J R Leong**[1]**, T Adams**[3,4]**, C Affeldt**[1]**,
A Bisht**[1]**, C Bogan**[1]**, J Degallaix**[5]**, C Gräf**[1,2]**, S Hild**[2]**,
J Hough**[2]**, A Khalaidovski**[1]**, N Lastzka**[1]**, J Lough**[1]**,
H Lück**[1]**, D Macleod**[3,6]**, L Nuttall**[3,7]**, M Prijatelj**[1,8]**,
R Schnabel**[1]**, E Schreiber**[1]**, J Slutsky**[1,9]**, B Sorazu**[2]**,
K A Strain**[2]**, H Vahlbruch**[1]**, M Wąs**[1,4]**, B Willke**[1]**,
H Wittel**[1]**, K Danzmann**[1]**, and H Grote**[1]

[1] Max-Planck-Institut für Gravitationsphysik (Albert-Einstein-Institut) und
Leibniz Universität Hannover, Callinstr. 38, D-30167 Hannover, Germany
[2] SUPA, School of Physics and Astronomy, The University of Glasgow, Glasgow,
G12 8QQ, UK
[3] Cardiff University, Cardiff CF24 3AA, United Kingdom
[4] Laboratoire d'Annecy-le-Vieux de Physique des Particules (LAPP), Université
de Savoie, CNRS/IN2P3, F-74941 Annecy-le-Vieux, France
[5] Laboratoire des Matériaux Avancés (LMA), IN2P3/CNRS, Université de
Lyon, F-69622 Villeurbanne, France
[6] Louisiana State University, Baton Rouge, LA 70803, USA
[7] Syracuse University, Syracuse, NY 13244, USA
[8] European Gravitational Observatory (EGO), I-56021 Cascina (Pi), Italy
[9] CRESST and Gravitational Astrophysics Laboratory NASA/GSFC,
Greenbelt, MD 20771, USA
[10] The University of Mississippi, Oxford, MS 38677, USA

E-mail: `kldooley@olemiss.edu`

Abstract. The German-British laser-interferometric gravitational wave detector GEO 600 is in its 14th year of operation since its first lock in 2001. After GEO 600 participated in science runs with other first-generation detectors, a program known as GEO-HF began in 2009. The goal was to improve the detector sensitivity at high frequencies, around 1 kHz and above, with technologically advanced yet minimally invasive upgrades. Simultaneously, the detector would record science quality data in between commissioning activities. As of early 2014, all of the planned upgrades have been carried out and sensitivity improvements of up to a factor of four at the high-frequency end of the observation band have been achieved. Besides science data collection, an experimental program is ongoing with the goal to further improve the sensitivity and evaluate future detector technologies. We summarize the results of the GEO-HF program to date and discuss its successes and challenges.

1. Introduction

GEO 600 is the German-British laser-interferometric gravitational wave (GW) detector with 1200 m long arms folded inside 600 m long beam tubes located near Hannover, Germany [1, 2, 3, 4]. Figure 1 shows a simplified optical layout of GEO 600, referred to throughout this paper.
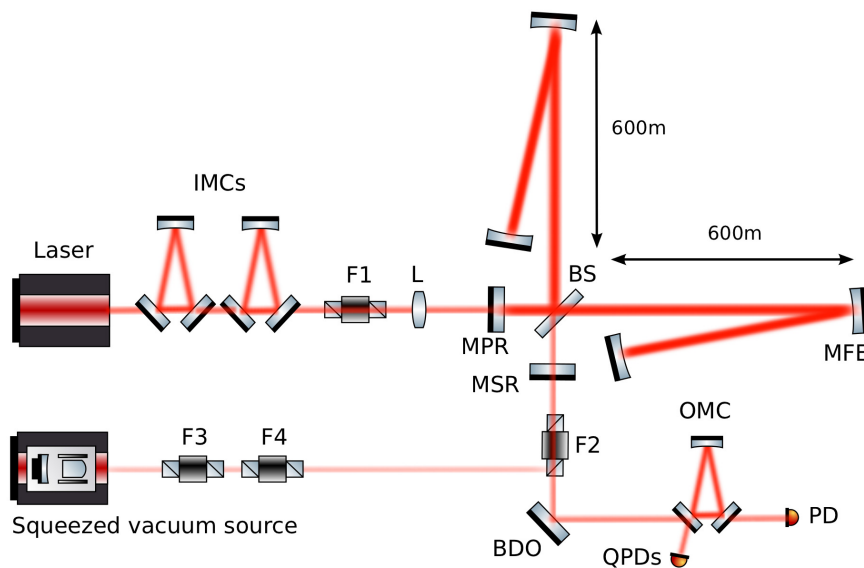
Figure 1. Simplified optical layout of GEO 600. IMCs: Input mode cleaners, F1, F2, F3, F4: Faraday isolators, L: Lens, MPR: Power recycling mirror, MSR: Signal recycling mirror, BS: beam splitter, MFE: East end mirror, BDO: Output beam director, OMC: Output mode cleaner, PD: Photodiode for DC readout, QPDs: Quandrant photodiode for squeezed field and OMC alignment.

The GEO 600 detector stood apart from its contemporary first-generation counterparts because of a significantly limited budget and the incorporation of more innovative but also riskier technologies [5]. After conducting science runs together with the other first-generation GW detectors, the GEO 600 detector continued to operate as a data-taking instrument with the LIGO Hanford 2 km interferometer in a program called Astrowatch from 2007 to 2009. During this time the other detectors in the network, LIGO and Virgo, were enhancing their 4 km and 3 km instruments, respectively. [6, 7]. Then, in 2009, an upgrade program called GEO-HF began with the goal of carrying out a series of upgrades to improve the detector's high-frequency (HF) shot-noise-limited sensitivity, around 1 kHz and above, and to demonstrate new technologies [8]. Simultaneously, GEO 600 was to serve as the GW community's Astrowatch detector, continuing to collect scientific data while the other detectors went offline for a 4–6 year period to construct and commission the so-called Advanced Detectors [9, 10]. GEO 600 thus operated as an observatory for large parts of the GEO-HF program, mandating substantial effort to maintain continuous operation. Not only did such effort facilitate the small chance of serendipitous discovery, but it also provided a unique opportunity to test new technologies in an observatory-style environment, setting GEO 600 apart from a standard laboratory setting.

This article explains the detector developments during the course of the GEO-HF program, reviewing the early upgrades that were reported in the latest update article [3] and are continuing to the present day. Section 2 begins with a review of the GEO-HF goals including the design noise curve and provides a summary of the accomplishments to date. Each of the upgrades is then discussed in more detail, including how they help accomplish the GEO-HF goals and the successes and
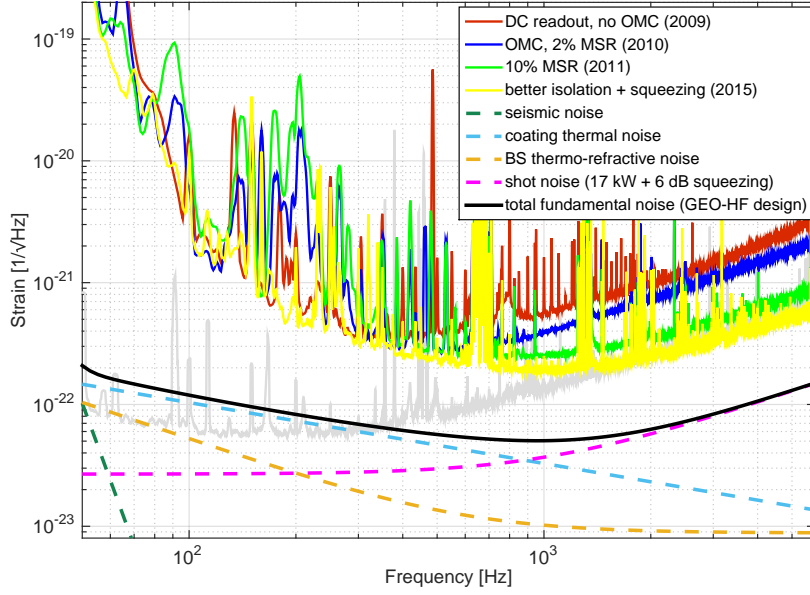
Figure 2. Progression of strain-equivalent noise curves upon completion of major milestones of the GEO-HF upgrade program compared to fundamental noise sources representing the goal sensitivity. A new signal recycling mirror, squeezed vacuum injection, and DC readout contribute to the substantial improvement in high-frequency sensitivity. The change to tuned signal recycling with DC readout was made early on in the GEO-HF program and is reflected in all of these curves. An increase in laser power is still a work in progress. The large cluster of lines centered around 650 Hz are the violin modes of the suspension fibers. Shot noise is plotted for the GEO-HF goals of 20 W input power (17 kW circulating) and 6 dB squeezing and MSR stands for signal recycling mirror. A strain noise curve for Virgo during the S6e science run is shown in light grey for comparison [11]. The thermo-refractive noise of the beam splitter (BS) is significant for GEO 600, since there are no arm cavities to reduce this effect.

challenges presented by each. Section 3 summarizes the overall current state of the detector, highlighting an up-to-date detector noise budget and challenges faced in moving forward. The potential effectiveness of GEO 600 as a GW detector and the tools developed to aid its operation as an observatory while carrying out installation and optimization work in parallel (called *commissioning*) are described in Section 4. Finally, Section 5 provides a summary and outlook.

2. GEO-HF Upgrades

The limiting fundamental noise sources for the GEO-HF design are plotted in Figure 2 and are compared to strain sensitivity curves highlighting selected upgrade milestones. The GEO-HF goal is to reach a sensitivity limited by fundamental shot noise and to maintain or improve low frequency sensitivity. The parameters that define the shot noise design curve are 20 W input power (17 kW circulating power), 6 dB of observed

squeezing (defined as the improvement of the shot-noise-limited sensitivity due to the application of squeezing), and tuned signal recycling with a signal recycling mirror of 90 % reflectivity. The following incremental upgrades to the baseline GEO 600 configuration are the cornerstones of the GEO-HF program:

- a transition from RF readout to DC readout, and the addition of an output mode cleaner (OMC).
- a change from detuned to tuned signal recycling and a replacement of the signal recycling mirror to one with higher transmission.
- the injection of squeezed vacuum into the detection port.
- an increase in laser power and measures supporting the operation at higher power.

To date, each of these upgrades has been partially or fully implemented and as much as a factor of 4 improvement in sensitivity above 600 Hz has been achieved. In the sections below we review the motivations [8] and present the implementation, results, and implications of each of the upgrades. The discussions are grouped by topic and do not necessarily reflect chronological order. Refer to Figure 8 for a timeline of major events during the GEO-HF program.

2.1. DC readout and implementation of an OMC

Amongst the first of the upgrades in the GEO-HF program was the change of the GW readout scheme from RF (heterodyne) to DC (homodyne) readout in 2009 [12]. DC readout provides a fundamental $\sqrt{3/2}$ improvement in sensitivity at shot-noise-limited frequencies due to the elimination of the cyclostationary shot noise of RF readout [13, 14]. It was also an important simplification for the implementation of squeezing because a squeezed light source needs to be prepared only in the audio band, rather than at both, audio and RF, frequencies. Moreover, DC readout significantly reduces the coupling of oscillator phase and amplitude noise to the GW signal [15]. Phase noise of the electronic RF oscillator and of the RF signal path had been a nearly limiting noise source for GEO 600 [3] with RF readout. With DC readout, the phase noise coupling to the GW readout was reduced by a factor of 50. DC readout also has disadvantages. Due to the presence of the TEM_{00} carrier field created by the dark fringe offset, alignment sensing errors for the main interferometer can be induced by beam motion on the alignment sensors. Stable locking with DC readout was possible only after a technique known as 2f-centering was developed, which actively stabilizes the beam on the alignment sensors, as further described in [3].

The introduction of an output mode cleaner (OMC in Figure 1) followed shortly thereafter in 2010 [16]. A four-mirror monolithic bow-tie cavity was installed in the interferometer's output beam path in a new vacuum tank separated by a window from the rest of the vacuum system for ease of access. An OMC, whether in conjunction with RF or DC readout, is necessary in order to achieve the best possible classical shot noise limit. This is because an OMC suppresses higher-order modes (HOMs) of the optical light field, which are originating from contrast defects within the main interferometer. When used with DC readout, an OMC also attenuates the RF modulation sidebands used to control auxiliary interferometer degrees of freedom. If the output field is not filtered, both higher-order modes and RF sidebands increase shot noise without contributing to the GW signal.

The stark effect that the OMC had on reducing GEO 600's high frequency noise floor can be seen in Figure 2. The trace labeled 'OMC, 2% MSR (2010)' can be

compared to the trace labeled 'DC readout, no OMC'. Both spectra were taken with the detector in tuned signal recycling mode with DC readout. Although the use of an OMC indeed improved high-frequency sensitivity, it initially degraded the GEO 600 sensitivity at lower frequencies. The root of the problem comes from the fact that higher-order modes in the frame of the OMC can couple into the GW signal via jitter of the output beam. The amplitude of the coupling is non-stationary and the spectral features around 90 Hz and 200 Hz and at nearby frequencies in trace 'OMC, 2% MSR' in Figure 2 were caused by this process.

Significant improvements in the low-frequency sensitivity achieved since the introduction of the OMC have come as a result of addressing the amount of jitter motion and its coupling to the readout. This includes an upgrade of the output optics' (BDO in Figure 1) suspensions to reduce beam jitter and an improvement of the vibration isolation of the OMC. Furthermore a 37% reduction in HOMs at the output port was achieved through thermal compensation of an astigmatism at the east end mirror (MFE in Figure 1), thus potentially decreasing coupling of HOMs to the GW channel as well [17]. The effects of these efforts is seen by comparing the low-frequency sensitivity of the curve in Figure 2 labeled 'better isolation' with those preceding it.

The development of an OMC alignment scheme in the presence of higher order modes and beam jitter is also critical for reducing the coupling of beam jitter and HOMs to the GW readout. Originally, a simple dither of the output optics' suspensions was used in a control scheme to maximize the power throughput of the OMC. However, because 80 % of the power at the GEO 600 output port is composed of HOMs, such a scheme may find an alignment that partially transmits HOMs rather than pure TEM_{00} light. A scheme that maximizes only the TEM_{00} light transmitted through the OMC came next by adding an audio frequency modulation to the carrier field [18]. The response of the GW readout (the optical gain) is maximized with such a double-demodulation scheme, but the signal-to-noise ratio (SNR) of these alignment signals is low and creates a significant limitation on the alignment control bandwidth. The newest technique, modulated differential wavefront sensing (MDWS), uses wavefront sensors in reflection of the OMC (QPDs in Figure 1) and has been recently commissioned [5]. The wavefront sensors sense the relative alignment between the interferometer RF sidebands representing the GW mode and audio sidebands generated from a length dither of the OMC representing the OMC eigenmode. This scheme both eliminates low frequency dithering of the output steering optics and facilitates an increase in the alignment control bandwidth up to several Hz, helping to reduce the non-stationary beam jitter coupling.

2.2. Signal recycling bandwidth increase

Other relatively early upgrades which enabled progress towards reaching the GEO-HF goals were related to the signal recycling cavity (SRC). An important step in the GEO-HF program was the reshaping of the shot noise by changing the finesse of the SRC and varying its operating point (detuning).

Prior to the GEO-HF upgrade, the signal recycling mirror (MSR in Figure 1) was held off-resonance from the carrier in order to maximally amplify one of the GW sidebands. In this state, known as detuned signal recycling, an increase in the GW signal-to-shot noise ratio is achieved in a band around a particular frequency at the expense of all other frequencies. From 2005 to 2009, GEO 600 used a detuning of

530 Hz. Early experiments showed that operating the signal recycling cavity in the detuned state was not optimal for GEO 600 due to technical noise couplings to the GW readout which could be significantly reduced in a tuned state where upper and lower GW sidebands are equally resonant [19]. Operation in a tuned state would not only improve the high-frequency sensitivity, but also open the path to being able to benefit from squeezing with a frequency-independent quadrature angle at all shot-noise-limited frequencies. In 2009, tuned operation of the signal recycling cavity was commissioned together with the change to DC readout [3]. All curves in Figure 2 use tuned signal recycling with DC readout. A comparison of the tuned and detuned cases is found in Ref. [19].

The use of tuned signal recycling is most appropriate if the bandwidth of the SRC is comparatively high. The build-up of the GW signal falls off as a Lorentzian with frequency, so a large improvement in high frequency sensitivity could therefore be achieved by decreasing the finesse of the SRC. This was accomplished in fall 2010 by exchanging the signal recycling mirror from one with a reflectivity of $R = 98\%$ to one with a reflectivity of $R = 90\%$. The cavity bandwidth increased from about 230 Hz to 1150 Hz. The trace labeled '10% MSR' in Figure 2 shows the result of the signal recycling mirror swap in comparison to the '2% MSR' trace. An improvement by a factor of more than 2 at high frequencies was achieved as planned.

The new signal recycling cavity's lower finesse had a number of negative side effects, though, which resulted in sensitivity setbacks at lower frequencies. The exaggeration of the peaks from 80 Hz to 1 kHz in the '10% MSR' trace in Figure 2 compared to before results largely from a reduction of the phenomenon known as mode healing [20]. With the lower MSR reflectivity, HOMs at the interferometer's output port are less effectively converted back into the interferometer's fundamental mode. The HOM content at the output port increased by about 50%. Given that HOMs are the means by which beam jitter couples to the GW readout and that beam jitter had not yet been reduced at the time of these spectra, the dominant reason for an increase in low-frequency noise was a higher coupling of jitter through the OMC.

Another side effect of the new signal recycling cavity's lower finesse was that it decreased the SNR of the SRC length signal, which is derived from 9 MHz resonant sidebands and the carrier light in the SRC. The result of a lower SNR signal while maintaining the same control bandwidth (35 Hz) is higher feedback noise. This is currently the limiting noise source from 50 Hz to 100 Hz, as will be discussed in Section 3.

2.3. Squeezing

Injection of squeezed vacuum states to the interferometer's output port is a novel technique employed to suppress quantum noise [21, 22] and is one of the technology demonstration highlights of the GEO-HF program. The GEO 600 squeezer was built at the Albert-Einstein-Institut in Hannover and transported to the site in April 2010 [23, 24]. Following installation and integration, a first successful demonstration of the high-frequency noise reduction was achieved in fall 2010 just prior to the signal recycling mirror swap. The sensitivity above approximately 1 kHz was improved by 3.5 dB and this accomplishment marked the first of its kind for large scale GW detectors [25]. A typical example of how squeezing helps achieve the GEO-HF goals can be seen by comparing the traces labeled 'squeezing' in Figure 2 to '10% MSR' at frequencies above approximately 700 Hz.
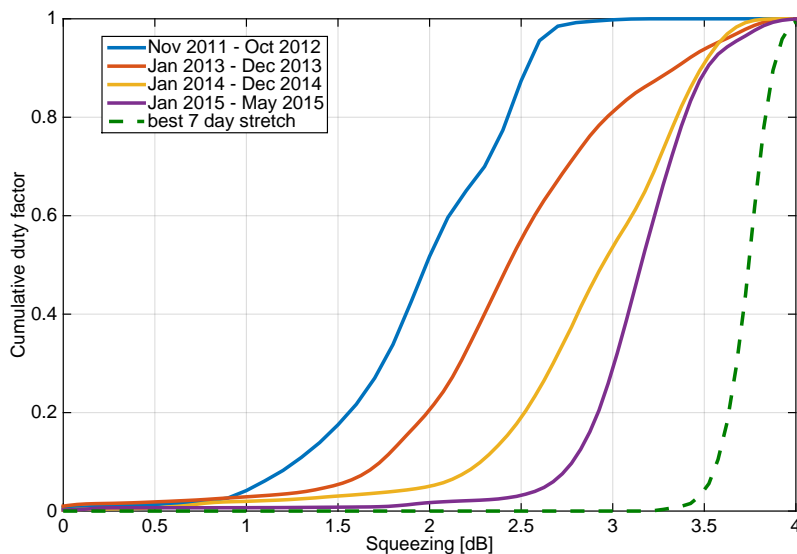
Figure 3. Record of the improvement of the observed squeezing level during the course of the last three and a half years. The cumulative duty factor while squeezing was applied illustrates for what fraction of time squeezing at a given level (and lower) was observed. (A cumulative duty factor of 0.5 corresponds to the median of the distribution.) Four consecutive periods of time are displayed. A 7 day example of a particularly stationary period is shown in order to demonstrate what can be achieved on shorter time scales. During all Astrowatch science times during this period, the squeezing up time was around 85 %.

The sensitivity gain from squeezing at GEO 600 is obtained without negative side effects, although data quality was initially compromised upon the squeezer's installation and some indirect noise contamination required mitigation efforts. The main challenges encountered were from the back-scattering of light into the interferometer mode from the additional optics required for squeezing and noise from control malfunctions of the squeezer. The scattering is mitigated through acoustic and vibrational isolation of the optics, and three Faraday isolators in the squeezing path including the injection Faraday, each of which provide approximately 40 dB of isolation (F2, F3, F4 in Figure **??**). This isolation is sufficient, but any reduction cannot be afforded. Additional controls implemented on optical and mechanical degrees of freedom both internal to the squeezer and on those relative to the main interferometer, in addition to other software enhancements, allow the squeezer to operate routinely and consistently without the introduction of spurious noises into the detector. An analysis of the data glitchiness with and without squeezing was performed in 2012 and shows that squeezing does not negatively affect the data quality [26].

Throughout the work on squeezing, the goals have been to ensure stable operation and to reach a high stable squeezing factor. The resulting progress is shown in Figure 3. The cumulative duty factor with squeezing is plotted for four consecutive periods of

time. Squeezing has been in near continuous use since fall of 2011 and in all has operated for 85% of the time during which the detector was in science mode. The average observed squeezing level has progressed by several tenths of a dB per year.

The development and commissioning of squeezer alignment and phase control systems has had top research priority and contributed to the improvements in Figure 3. A wavefront sensing alignment scheme in reflection of the OMC was designed to ensure maximum overlap of the squeezed vacuum field with the interferometer output field [27]. It operates with a bandwidth of up to several Hertz and is important for long-term stability of the squeezing level. In addition, a new error signal derived in transmission of the OMC was devised for sensing the relative phase of the squeezed field with the interferometer output. It eliminates lock point offsets due to HOMs that had previously created a fluctuating squeezing level [28]. Both the new alignment and phase control schemes have been commissioned and are in continuous use.

A new focused research effort is now underway to reduce the optical losses. The optical losses in the GEO 600 squeezer path amount to approximately 40%, and are the dominant limitation on the potential sensitivity improvement from squeezing. The losses alone reduce the maximum possible observed squeezing from 10 dB to 4 dB. The poor optical efficiency results quite easily from the sum of many small losses, including the 8 passes through polarizing beam splitters, OMC internal losses, imperfect mode matching to the OMC, and photodetector quantum efficiency. Carefully addressing each of these loss sources to reduce the total losses to 20% is a near-term goal. Phase noise also contributes to reducing the maximum possible squeezing level. It has been measured to be about 37 mrad rms and reduces GEO 600's best observed squeezing by about 0.2 dB. The record to date is an improvement of the shot-noise-limited strain sensitivity by 3.7 dB, the equivalent to a laser power increase by a factor 2.3 [26].

2.4. Power increase

The planned power increase has proven to be the hardest of the GEO-HF goals to meet. An increase from 2 kW circulating power to approximately 17 kW (20 W input power) should provide a factor of about 3 improvement in sensitivity at frequencies limited by shot noise (which should be 900 Hz and above, in the absence of technical noise sources). To date, stable operation of the detector with up to 4 kW circulating power has been achieved and the corresponding expected high-frequency sensitivity improvement observed. However, due to increasing noise of unknown origin at frequencies below about 1 kHz, this higher power state is not yet used in standard running conditions as is discussed in Section 3.

A number of hardware upgrades had to be carried out to ensure the availability of at least 17 kW circulating power. These upgrades began in fall 2011 with the installation of a 35 W laser system, to replace the previous 12 W laser. The new system consists of a laser-diode-pumped Nd:YAG master laser and a subsequent Nd:YVO$_4$ amplifier stage [29, 30]. The following fall, a vacuum incursion took place to replace several components of the input optics chain to ensure high-power compatibility. The LiNbO$_3$ crystals used in the electro-optic modulators (EOMs) were replaced with RTP crystals that have more than twice the damage threshold and a lower thermal lensing effect [31]. Four of the six input mode cleaner mirrors were replaced to reduce the finesse of the cavities in order to improve their transmission and ease the locking. In addition, the in-vacuum mode matching telescope was adjusted to preemptively compensate for thermal lensing that would result from power absorption at high
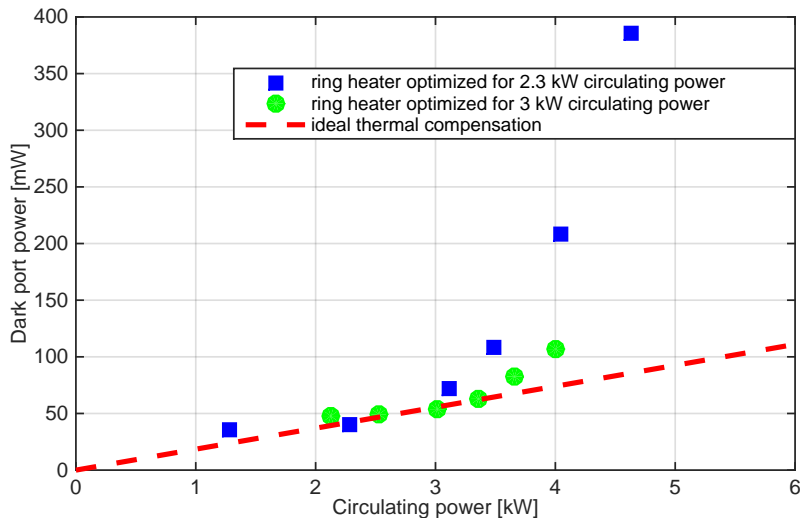
Figure 4. Measurement data demonstrating the fundamental reason for the difficulty in increasing the laser power in GEO 600. A power-dependent thermal lens in the BS results in an increase of higher-order modes at the output port which in turn leads to a breakdown of interferometer control. Indirect compensation of the BS thermal lens through a radius of curvature adjustment of the east arm's folding mirror offers some relief. The dashed red line shows the expected dark port power if the BS thermal lens could be fully compensated. A constant contrast defect of 18 ppm is assumed.

power in the input chain Faraday isolators and EOMs [33]. To facilitate this, an interchangeable lens (L in Figure 1) on a suspended bench was replaced, after it was found with optical simulations that the previous choice of lens was not optimal for high-power operation. The thermal lens effect to be expected from the Faraday isolator (F1) was measured in the laboratory, and served as input for the optical simulations.

A challenge in achieving higher power operation which was addressed early on in the GEO-HF program was that the signals on the individual optics' local position sensors were contaminated by scattered light from the main interferometer. The amount of scattered light increases proportional to the circulating power in the main interferometer optical mode and would thus inject more and more false position information to the local velocity damping servos as the power would increase. As a result, the interferometer became more instable for higher circulating power and would eventually lose lock. The elimination of stray light coupling was achieved through the implementation of a modulation-demodulation technique for the local position sensors [33]: In this scheme, the currents of the light emitting diodes of these sensors are modulated at single frequencies around 7-10 kHz. The photocurrents of the adjacent photodiodes are coherently demodulated and this signal serves as the error signal for the velocity damping servo.

The single most critical limitation to operating GEO 600 with higher laser power is a strong thermal lens at the beam splitter (BS). Because GEO 600 does not

have Fabry-Perot arm cavities, all of the circulating power in the interferometer is transmitted through the substrate of the BS, whose absorption has been measured to be 0.5 ppm/cm [5]. Furthermore, due to the beam's non-normal angle of incidence on the BS, the resulting lens is elliptical and more challenging to compensate. The severity of the uncompensated thermal lens is highlighted in Figure 4 which shows measurements of the quadratic increase of power at the output port as a function of power at the BS due to contrast defect. In the case of a perfectly compensated thermal lens, the relationship should be linear.

Partial, indirect compensation of the BS thermal lens is accomplished through the use of a radiative ring heater behind the far east mirror which had been installed in 2003 to correct for the mirror's slightly incorrectly manufactured radius of curvature [32]. The data points in Figure 4 show that optimal ring heater powers that compensate the BS thermal lens can be found for up to 3 kW circulating power. Exploration of optimal ring heater powers for higher circulating power levels has been challenging because of the time required for thermal equilibrium to be reached and because of an increasing lack of detector stability. For circulating powers beyond about 3.5 kW, the excess output port power increases the shot noise on the many auxiliary sensing photodiodes, and contributes to a break-down of control and loss of lock.

A next step in the series of work required to achieve higher laser power for GEO-HF is to install a thermal compensation system directly at the BS. An array of heating elements has been designed to project optimized patterns of radiation onto the BS. Initial results have demonstrated a 30 % reduction of thermally induced HOMs and commissioning is ongoing.

3. Noise budget and challenges

Figure 5 shows the current status of the understanding of GEO 600's technical and fundamental noises. This snapshot was taken during a night of standard Astrowatch operation with 2 kW circulating power and 3.2 dB of observed squeezing. The dashed lines are the analytical models of fundamental noise sources as presented in Fig. 2 and the solid lines are actual data. The noise projections are created from continuously measured data and recorded coupling transfer functions [34]. To aid commissioning, the noise budget is updated in near real time once every few seconds. The transfer functions that are used to make the projection are updated periodically. The laser frequency stabilization control loop and the SRC length control loop have calibration lines to enable real-time tracking and adjustment of the magnitude of the corresponding noise coupling transfer functions. The uncorrelated sum of the fundamental and technical noise sources can be compared to the measured strain sensitivity and shows that the GEO 600 noise floor is well understood at low and high frequencies. However, between 100 Hz and 1.5 kHz there is unexplained noise.

Below 100 Hz, strain sensitivity is dominated by technical control noises. One reason for the control noises being high is that there is only very limited seismic pre-isolation. The control loops therefore need comparatively high bandwidth to keep the interferometer sufficiently quiet. The alignment control loops and the signal recycling cavity length control loop are the most severe sources of noise impression below 100 Hz. The wavefront sensors that derive the Michelson alignment signals are at the output port of the interferometer and have a noise floor at high frequencies dominated by shot noise from higher order modes. Below approximately 100 Hz, these signals are limited by beam jitter noise coupling on the associated wavefront sensors. Unity gain
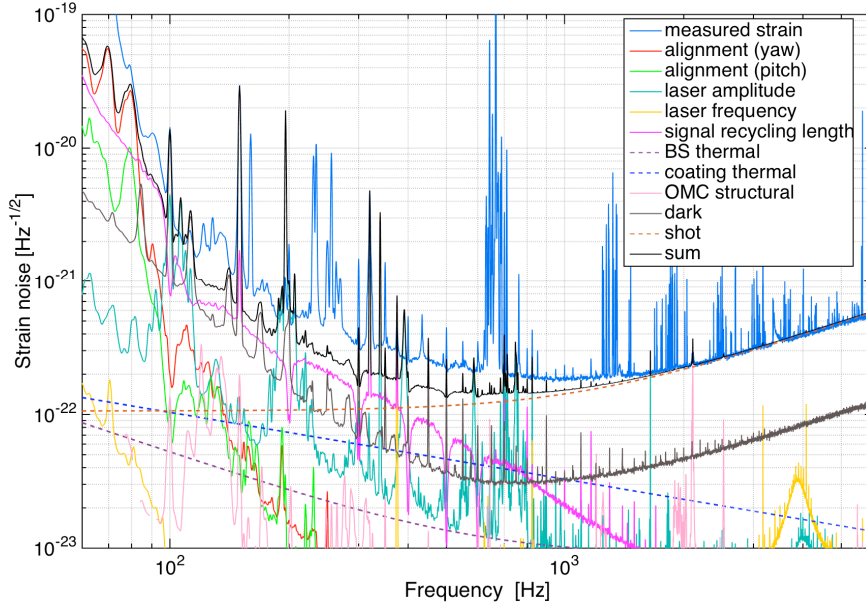
Figure 5. Noise budget of GEO 600 with 2 kW circulating power and 3.2 dB observed squeezing. The blue curve is the measured amplitude spectral density of the strain-equivalent noise (also called sensitivity throughout the paper). The dashed lines represent analytical models of fundamental noise sources and the solid lines are actual data. The uncorrelated sum of fundamental and technical noise sources explains the GEO 600 sensitivity both above 1.5 kHz and below 100 Hz. Excess noise in the mid-frequency band remains unexplained.

frequencies of about 5 Hz are necessary for these loops to have enough low-frequency gain to control the pitch and yaw modes of the suspensions. The SRC length loop has a bandwidth of 35 Hz such that (shot-noise limited) feedback noise is a factor of a few below the strain noise floor. Partial cancellation of this noise with a feed-forward scheme proved difficult, as the level of the signal recycling mirror length noise coupling to strain varies with output beam alignment onto the OMC. The process is the same as for the beam jitter coupling in conjunction with higher order optical modes, as described in Section 2.1.

The strain sensitivity at high frequencies is dominated by shot noise. The next most significant contributor, dark noise from the readout electronics, is a factor of 7 below shot noise without squeezing, but is only a factor of 4.5 below shot noise with squeezing engaged, as shown in Figure 5. Work is ongoing in implementing a new electronics design to decrease dark noise by a factor of 2 to 3 in order to increase the level of observable squeezing. Laser amplitude and frequency noise are not always stationary and they sometimes start to affect the sensitivity at several kHz, as can be seen in this example from the laser amplitude noise peak at 4 kHz ‡.

In the search for the culprit of the excess mid-frequency noise, many potential sources of technical noise have been ruled out. This includes saturations at both RF and DC of sensing photodiodes. Scattered light has been systematically searched for

---

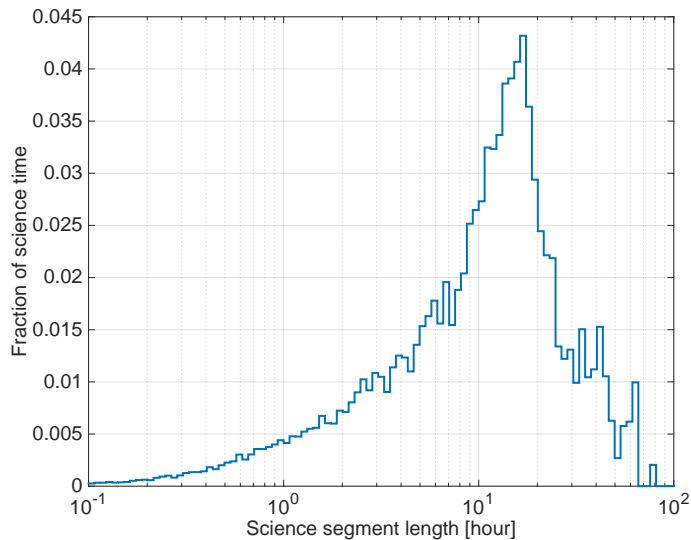‡ The cause for this non-stationarity is under investigation.

Figure 6. Histogram of the fraction of science time spent in a lock of a given length during Astrowatch times from 2008 through 2014. The total duration is 38400 hours or 4.4 years, resulting in a 63 % average science time duty factor.

through extended tapping tests for acoustic coupling via acoustic excitation of vacuum chambers and associated optics. Filter experiments have ruled out scattering from sources external to the vacuum system. Suspended baffles were installed around the east arm's end test mass and the two main test masses in the central area to rule out small-angle scattering. Efforts to think about potential additional fundamental noise sources has in fact resulted in an updated thermal noise model for GEO 600 because of a stripe pattern (caused by the folded arm geometry of GEO 600) on the far end mirrors that had not been previously considered [35]. As a result of this investigation, the theoretical coating thermal noise curve has been adjusted to be 20% higher than in the last update article, but is still too far below the noise floor to explain the observed strain-equivalent noise. Furthermore, the amount of excess noise is not stationary and studies to determine the time scale of its changing amplitude produce varying results.

As mentioned in Section 2.4, operation with 4 kW circulating power can be achieved during commissioning periods. Operation with 2 kW to 2.5 kW is standard, however, because the increase in laser power brings with it an increase in noise below 600 Hz. The shape of the excess noise is $1/f$ and despite systematic investigations to identify its cause, this problem has not yet been solved. An increase in laser power remains the last of the GEO-HF goals to be carried out and hinges on successful implementation of direct thermal compensation at the beam splitter and uncovering the source of the power-dependent mid-frequency noise.

4. GEO 600 as a GW detector

An integral aspect of the GEO-HF program was not only the series of upgrades to improve the sensitivity at high frequency, but also GEO 600's status as a GW detector. The standard mode of operation during the last 6 years has been for commissioning activities to take place during the day and for GEO 600 to operate in Astrowatch mode during the nights and weekends. An exception was the period from June to August 2011 when GEO 600 participated in a dedicated data-taking run (known as S6e or VSR 4) with the French-Italian detector, Virgo. At this time, the GEO-HF upgrades that had already taken place resulted in GEO 600's sensitivity above 2 kHz equalling that of the Virgo detector, as can be seen in Figure 2 (light grey curve) [36].

In all, during the 7 years between 2008 and 2015, 63% of the time was spent collecting science quality data. The achievement of this high duty factor is possible because of the detector reliability which results in long continuous lock stretches and because of the success of automatic re-locking which requires human intervention on average only once every five days. Figure 6 shows a histogram of lock stretch lengths during the course of the GEO-HF upgrade program. The median segment duration is 11.5 hours and the longest lock stretch to date occurred in early January 2015 and was 102.5 hours long. Despite this reliability, time and care was needed to achieve this consistently high duty factor. Maintenance of the aging hardware as well as the time needed for the commissioning of new interferometer configurations both reduce the time available for observation. Simultaneously, ensuring that the data produced were of high quality and accurate calibration was made complicated by changes to the underlying instrumentation. These challenges inspired tools and analysis techniques that rapidly evaluated the effect on sensitivity and likely origin of instrumental noises to help inform commissioning improvements and maintain a sensitive, stable detector.

The primary GW source candidates for GEO 600 are gamma ray bursts (GRBs) or their progenitors, and supernovae (SNe), both of which produce short burst-like signals at high frequencies. The sensitivity of the detector to such sources depends not only on the time-averaged level of the detector noise floor, but also on the degree of Gaussianity of the detector noise. A putative GW burst signal must be evaluated in the context of the background of instrumentally produced transients that would trigger the same search. A focus was placed on the development of monitors and figures of merit (FOMs) that track the stationarity of the GEO 600 data and make it easily accessible to the instrument commissioners. One example is the transient-noise visualizer, called Omegamap [38], developed to provide information complementary to that encoded in the amplitude spectral density. Whereas a spectrum assumes stationarity of the data, the Omegamap time-frequency representation emphasizes the deviations from that stationarity. The Omegamap is related to a normalized spectrogram, but is one in which all FFT length choices are included and ranked by significance, allowing the observation of transients of any time-frequency character.

Prompt and thorough accessibility to data quality monitoring and detector performance was realized through the development of an improved version of the overview web pages that had been used in the initial detector era. These 'summary pages' are built upon a new universal architecture based on the computer cluster infrastructure used by GW scientific collaborations for data analysis of the full detector network data. This enhances the portability of monitor tools development and ensures functionality into the future. The summary pages organize and present monitors in a concise manner via standard web servers. Month-long and daily summaries of the
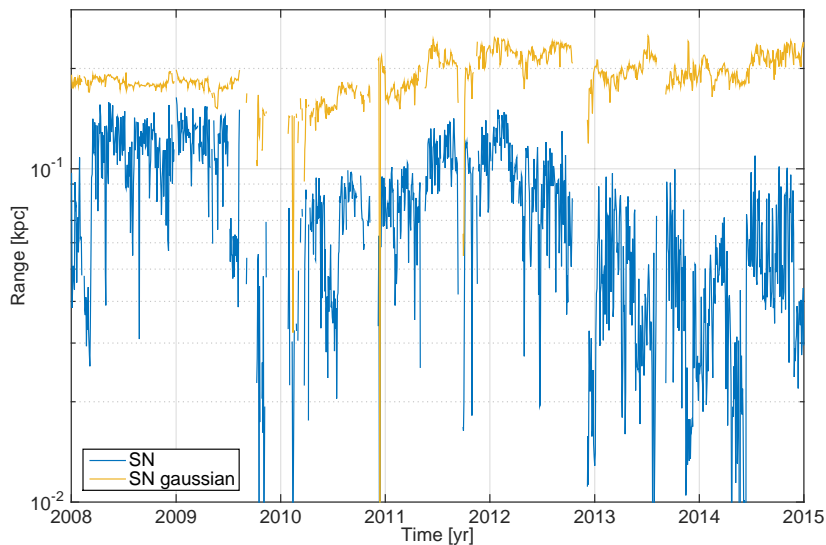
Figure 7. Figures of merit tracking the astrophysical reach of GEO 600 during GEO-HF. The blue trace shows the distance out to which GEO 600 could detect GWs from a binary neutron star inspiral upon averaging over all BNS orientations. The red trace shows the range to which a supernova could be detected. It takes into account not only the time-averaged noise floor, but also the glitchiness of the data.

detector's state are easily navigable and can be generated for any GW detector [37]. Other examples of new monitors that were developed during GEO-HF include the live noise budget presented in Sec. 3 as well as a real-time squeezing estimator. This vital connection between the detector data quality and commissioning activities led to a novel analysis framework for evaluating the cost-benefit of carrying out particular commissioning activities rather than keeping the detector in observation mode [38].

Figure 7 shows the time series of two FOMs for the astrophysical sensitivity of GEO 600. They both present the range to which GEO 600 could detect a supernova (SN). The dark yellow trace, similar to the binary neutron star inspiral range commonly used by the global network of detectors, is calculated from the time-averaged detector noise floor weighted for this type of source. It assumes Gaussian noise and uses a detection threshold with a SNR of 8. The blue trace uses the same averaged noise floor but adds information from the transient noise characteristics of the data. This non-Gaussian SN range is one of the most important new FOMs developed during GEO-HF. It allows for a more versatile estimate of possible analysis reaches and can be used to guide commissioning to focus on improving the transient noise characteristics of a detector [39]. This new FOM was adapted to sources such as GRBs or SNe, and it can be tailored for inspiral searches as well. In order to assure accuracy of these traces with respect to the astrophysics, calibration of the data was provided through real-time parameter tracking and an occasional absolute
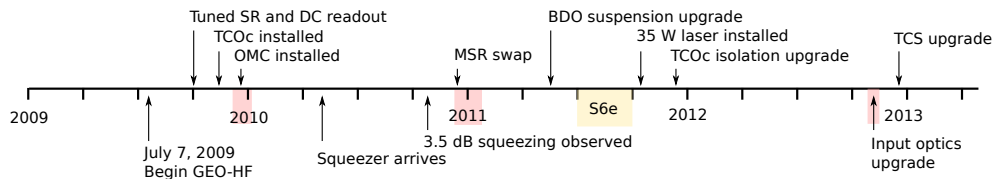
Figure 8. Timeline of major events during the GEO-HF program. GEO-HF officially started when the Enhanced LIGO detectors began their S6 science run on July 7, 2009. Tuned signal recycling (SR) together with DC readout were the first upgrade items to be implemented, followed by installation of the output mode cleaner (OMC), squeezing, signal recycling mirror (MSR) swap, and finally, steps required to increase the laser power. During this time, upgrades of the output chain seismic isolation (BDO suspension) also took place to reduce technical noises that became more prominent. In all, during the GEO-HF period, 63% of the time was spent collecting Astrowatch data, which includes a short science run with Virgo called S6e. TCOc: detection chamber containing the OMC; TCS: thermal compensation system.

calibration [5, 40].

During the course of the GEO-HF upgrades, the Gaussian SN range improved by about 20 %. At the end of the time period reported here, this range reached 220 pc, which reaches out to the star Betelgeuse. The large sensitivity increase seen above 2 kHz in Figure 2 is not reflected here because the SN ranges integrate frequencies between 500 Hz and 4 kHz with a stronger emphasis on the lower frequencies. The progression of the non-Gaussian SN range is much more variable and does not reach above 150 pc. It largely reflects the non-stationarity of the data and highlights the difficulty of achieving data Gaussianity, in particular with ongoing detector configuration changes and commissioning.

Several distinct commissioning epochs can be observed in Figure 7. After implementing DC readout and the OMC in late 2009, both SN ranges drop due to the fact that DC readout created an increased noise floor and glitches, in part from the beam jitter coupling described in Section 2.1. To mitigate this, the output optics suspensions were improved in May 2011. A small gap in the range data at this time is then followed by an improvement in sensitivity as seen by both FOMs. Directly after the output optics suspension upgrade and until March 2012, effort was put into eliminating some of the transient noise features at mid-frequencies from 100 Hz to 1 kHz. The result of this work is just barely visible in the non-Gaussian SN range. In 2012 several new glitch families began limiting the non-Gaussian SN range, and a number of them have not been successfully tracked down. The severe drop in the non-Gaussian SN range in November 2012 came after the input optics upgrade. The new input mode cleaner has a lower finesse, and therefore less passive filtering of laser frequency noise, which resulted in saturation of the laser frequency detection electronics. Fixing that is the improvement between December 2012 and January 2013. In all, it is clear that it is essential to constantly expend commissioning effort to maintain the astrophysical sensitivity by hunting for glitches and other noise sources which are constantly arising.

To date, no GW detections have been reported with GEO 600 or any other interferometric GW detector. No interesting candidate events from electromagnetic observations of nearby inspiraling neutron star binaries or from galactic core-collapse supernovae have occurred during the Astrowatch period. Gamma ray bursts, however,

triggered a coherent burst analysis for GWs associated with 129 GRBs between 2006 and 2011 using data from GEO 600 and one of the LIGO or Virgo detectors. This was the first GW analysis performed using data from a GW detector using squeezed-light states to improve its sensitivity. No evidence for GW signals was found with any individual GRB in the sample or with the population as a whole [36].

5. Summary and outlook

The GEO-HF upgrade program started in 2009, and by today most of the planned items have been successfully implemented. The shot-noise-limited sensitivity has improved by up to a factor of 4, and up to 3.7 dB of squeezing have been achieved. Work remains to be done reaching even higher squeezing levels and potentially increasing the circulating laser power. Besides these items GEO 600 has also served successfully as a data-taking instrument to fill the observational gap of larger observatories during their upgrades to advanced detectors. Since 2008, more than 4 years worth of data have been collected, allowing for serendipitous discovery in case of a nearby GW source. On top of this, GEO 600 always served and serves as a testbed for novel technology, making use of the fact that technologies can be tested in an observatory environment. A number of resulting contributions to the field have been referred to throughout this paper, such as thermal compensation, squeezing application and control, and software monitors to aid commissioning.

LIGO detectors approach their first observational run late in 2015, but nevertheless there will be observational gaps over the coming years in the LIGO-Virgo network. For the imminent future we therefore intend to operate GEO 600 in a similar fashion as to now, maintaining a reasonable fraction of observing time, and continuing to test technology. The large longer-term future of GEO 600 still has to be determined.

Acknowledgements

References

[1] Willke B *et al.* 2002 *Classical and Quantum Gravity* **19** 1377+ URL http://dx.doi.org/10.1088/0264-9381/19/7/321
[2] Grote H 2008 *Classical and Quantum Gravity* **25** 114043+ URL http://dx.doi.org/10.1088/0264-9381/25/11/114043
[3] Grote H and the LIGO Scientific Collaboration 2010 *Classical and Quantum Gravity* **27** 084003+ URL http://dx.doi.org/10.1088/0264-9381/27/8/084003
[4] Dooley K L and the LIGO Scientific Collaboration 2015 *Journal of Physics: Conference Series* **610** 012015+ URL http://dx.doi.org/10.1088/1742-6596/610/1/012015
[5] Affeldt C *et al.* 2014 *Classical and Quantum Gravity* **31** 224002+ URL http://dx.doi.org/10.1088/0264-9381/31/22/224002
[6] Smith J R and the LIGO Scientific Collaboration 2009 *Classical and Quantum Gravity* **26** 114013+ URL http://dx.doi.org/10.1088/0264-9381/26/11/114013

[7] Acernese F *et al.* 2008 *Journal of Optics A: Pure and Applied Optics* **10** 064009+ URL http://dx.doi.org/10.1088/1464-4258/10/6/064009

[8] Lück H *et al.* 2010 *Journal of Physics: Conference Series* **228** 012012+ URL http://dx.doi.org/10.1088/1742-6596/228/1/012012

[9] The LIGO Scientific Collaboration *et al.* 2015 *Classical and Quantum Gravity* **32** 074001+ URL http://dx.doi.org/10.1088/0264-9381/32/7/074001

[10] Acernese F *et al.* 2015 *Classical and Quantum Gravity* **32** 024001+ URL http://dx.doi.org/10.1088/0264-9381/32/2/024001

[11] URL https://wwwcascina.virgo.infn.it/MonitoringWeb/General/index.html?index_monitoring.html

[12] Hild S *et al.* 2009 *Classical and Quantum Gravity* **26** 055012+ URL http://dx.doi.org/10.1088/0264-9381/26/5/055012

[13] Gea-Banacloche J and Leuchs G 1987 *Journal of Modern Optics* **34** 793–811 URL http://dx.doi.org/10.1080/09500348714550751

[14] Niebauer T M, Schilling R, Danzmann K, Rüdiger A and Winkler W 1991 *Physical Review A* **43** 5022–5029 URL http://dx.doi.org/10.1103/physreva.43.5022

[15] Fricke T *et al.* 2012 *Classical and Quantum Gravity* **29** 065005+ (*Preprint* 1110.2815) URL http://arxiv.org/abs/1110.2815

[16] Prijatelj M *et al.* 2012 *Classical and Quantum Gravity* **29** 055009+ URL http://dx.doi.org/10.1088/0264-9381/29/5/055009

[17] Wittel H *et al.* 2014 *Classical and Quantum Gravity* **31** 065008+ URL http://iopscience.iop.org/0264-9381/31/6/065008/pdf/cqg_31_6_065008.pdf

[18] Smith-Lefebvre N, Ballmer S, Evans M, Waldman S, Kawabe K, Frolov V and Mavalvala N 2011 *Opt. Lett.* **36** 4365–4367 URL http://dx.doi.org/10.1364/ol.36.004365

[19] Hild S, Grote H, Hewitson M, Lück H, Smith J R, Strain K A, Willke B and Danzmann K 2007 *Classical and Quantum Gravity* **24** 1513–1523 URL http://dx.doi.org/10.1088/0264-9381/24/6/009

[20] Strain K A and Meers B J 1991 *Physical Review Letters* **66** 1391–1394 URL http://dx.doi.org/10.1103/physrevlett.66.1391

[21] Caves C M 1980 *Physical Review Letters* **45** 75–79 URL http://dx.doi.org/10.1103/physrevlett.45.75

[22] Schnabel R, Mavalvala N, McClelland D E and Lam P K 2010 *Nature Communications* **1** 121+ URL http://dx.doi.org/10.1038/ncomms1122

[23] Vahlbruch H, Khalaidovski A, Lastzka N, Gräf C, Danzmann K and Schnabel R 2010 *Classical and Quantum Gravity* **27** 084027+ URL http://dx.doi.org/10.1088/0264-9381/27/8/084027

[24] Khalaidovski A 2011 *Beyond the Quantum Limit: A Squeezed-Light Laser in GEO600* Ph.D. thesis Leibniz University Hannover

[25] The LIGO Scientific Collaboration 2011 *Nat Phys* **7** 962–965 URL http://dx.doi.org/10.1038/nphys2083

[26] Grote H, Danzmann K, Dooley K L, Schnabel R, Slutsky J and Vahlbruch H 2013 *Physical Review Letters* **110** 181101+ URL http://dx.doi.org/10.1103/physrevlett.110.181101

[27] Schreiber E, Dooley K L, Vahlbruch H and Grote H 2014 *Optics Express* Schreiber E, Dooley K L, Vahlbruch H, Affeldt C, Bisht A, Leong J R, Lough J, Prijatelj M, Slutsky J, Was M, Wittel H, Danzmann K, and Grote H, 2015 arXiv:1507.06468 (submitted to Optics Express)

[28] Dooley K L, Schreiber E, Vahlbruch H, Affeldt C, Leong J R, Wittel H and Grote H 2015 *Opt. Express* **23** 8235–8245 URL http://dx.doi.org/10.1364/oe.23.008235

[29] Frede M, Schulz B, Wilhelm R, Kwee P, Seifert F, Willke B and Kracht D 2007 *Opt. Express* **15** 459–465 URL http://dx.doi.org/10.1364/oe.15.000459

[30] Kwee P *et al.* 2012 *Opt. Express* **20** 10617–10634 URL http://dx.doi.org/10.1364/oe.20.010617

[31] Bogan C, Kwee P, Hild S, Huttner S H and Willke B 2015 *Optics Express* **23** 15380+ URL http://dx.doi.org/10.1364/oe.23.015380

[32] Lück H, Freise A, Goßler S, Hild S, Kawabe K and Danzmann K 2004 *Classical and Quantum Gravity* **21** S985+ URL http://dx.doi.org/10.1088/0264-9381/21/5/090

[33] Affeldt C 2014 *Laser Power Increase for GEO600* Ph.D. thesis Leibniz Universität Hannover

[34] Smith J R, Ajith P, Grote H, Hewitson M, Hild S, Lück H, Strain K A, Willke B, Hough J and Danzmann K 2006 *Classical and Quantum Gravity* **23** 527+ URL http://dx.doi.org/10.1088/0264-9381/23/2/016

[35] Heinert D, Craig K, Grote H, Hild S, Lück H, Nawrodt R, Simakov D A, Vasilyev D V, Vyatchanin S P and Wittel H 2014 *Phys. Rev. D* **90** 042001+ URL http://journals.aps.

org/prd/abstract/10.1103/PhysRevD.90.042001

[36] Collaboration L S and Collaboration V 2014 *Physical Review D* **89** 122004+ URL http://journals.aps.org/prd/abstract/10.1103/PhysRevD.89.122004
[37] URL https://atlas1.atlas.aei.uni-hannover.de/~geodc/LSC/monitors/
[38] Adams T *et al.* 2015 *Classical and Quantum Gravity* **32** 135014+ URL http://dx.doi.org/10.1088/0264-9381/32/13/135014
[39] Was M, Kalmus P, Leong J R, Adams T, Leroy N, Macleod D M, Pankow C and Robinet F 2014 *Classical and Quantum Gravity* **31** 085004+ URL http://dx.doi.org/10.1088/0264-9381/31/8/085004
[40] Leong J R *et al.* 2012 *Classical and Quantum Gravity* **29** 065001+ URL http://dx.doi.org/10.1088/0264-9381/29/6/065001